Flowing resistance and dilatancy of dense suspensions: lubrication and repulsion

Pierre Rognon, Itai Einav, Cyprien Gay

Flowing resistance and dilatancy of dense suspensions: lubrication and repulsion

Pierre Grégoire Rognon[1], Itai Einav[1] and Cyprien Gay[2]
[1] *School of Civil Engineering, J05, The University of Sydney, Sydney, New South Wales 2006, Australia*
[2] *Matière et Systèmes Complexes, Université Paris-Diderot - Paris 7, CNRS UMR 7057 - Paris, France*
(Dated: 17 December 2010)

We examine the flow properties of dense suspensions whose particles interact by viscous lubrication and surface repulsion. Using Soft Dynamics, we simulate its response to shear, prescribing the shear rate and the normal stress. We show that the behavior of steady flows can be described like that of dry grains, with a friction law and a dilatancy law. Their combination conveniently avoids the usual divergence of viscosity when approching the maximum packing fraction. However, the parameters of these laws depend in a non-trival way on the typical distance below which surfaces repel each other. The analysis of internal distribution of forces suggests a simple scenario underpining these complex dependencies. Pairs of particles appear to exchange a comparable lubrication force irrespective of their distance. This leads to a robust dynamic connected network controlling the collective resistance to flow.

PACS numbers: 83.80.Fg, 47.57.Gc, 83.80.Hj, 82.70.Kj

I. INTRODUCTION

Granular suspensions, emulsions, foams and blood share a similar microstructure: they are composed of individual particles immersed in a viscous fluid. Their flowing properties are pivotal in various practical issues, such as landslide mitigation, treatment of some cardiovascular diseases, fresh concrete settling or industrial food handling. A few decades of research have evidenced many of their rheological properties, but some great challenges still remain. The flowing behavior of immersed particles in *dense configurations* is one of them, as highlighted in many recent reviews [5, 6, 13–15, 21].

Many experimental and numerical studies measured the shear resistance to steady flow of dense suspensions. Most often, the particle concentration ϕ is selected prior to the experiment and would not vary. The material is then subjected to an imposed shear rate $\dot{\gamma}$ and the shear stress τ is measured, or *vice-versa*. Both methods highlight a flowing law in the form $\tau = \eta^{\text{eff}}(\phi)\dot{\gamma}$; with an effective viscosity η^{eff} that increases with ϕ and diverges at some maximum concentration ϕ_m. Many data satisfy the empirical Krieger-Dougherty law, $\eta^{\text{eff}} = \eta(1-\phi/\phi_m)^{-n}$, η being the viscousity of the surrounding liquid [3, 8, 11, 16, 21]. To date, the exponent n has not been given any clear physical meaning, yet the values that fit the data vary only slightly around $n \approx 2$. By contrast, the maximum concentration ϕ_m has a clear physical meaning: in order for the material to be sheared, the particles need some free space to avoid each other. The maximum concentration of spherical, mono-dispersed and rigid particles can be deduced from geometrical analysis. However, such an estimate may be difficult for polydispersed, not perfectly rigid or non-spherical particles [2]. For dense systems, this uncertainty has a critical impact on the viscosity prediction due to the divergent form of $\eta(\phi)$. In practice, the knowledge of the particle concentration is not sufficient to accurately infer the viscosity of the material.

An alternative approach has been recently introduced to express the flowing law of dense granular materials without liquid [7, 9, 10, 13]. Experiments and simulations were not performed under constant volume conditions, but rather under constant normal confining stress σ, allowing the material to dilate or contract. This loading mode corresponds, for instance, to free surface flows down a slope. The behavior of the material can then be expressed by a *friction law* and a *dilatancy law*. To a first order approximation in $\dot{\gamma}$, they read:

$$\frac{\tau}{\sigma} \approx \mu_s + bt\dot{\gamma}. \tag{1}$$

$$\phi \approx \phi_s - ct\dot{\gamma}. \tag{2}$$

Here, t is a time scale, discussed below, and μ_s, b, ϕ_s and c are numerical constants that depend on the nature of the grains, for instance their friction coefficient [7] and their possible cohesion [20]. This flowing behavior is similar to that of a Bingham fluid: it involves a critical shear stress $\tau_y = \mu_s\sigma$ below which there is no flow, and an effective viscosity $\eta^{\text{eff}} = b\sigma t$. Unlike for a Bingham fluid, however, both the critical shear stress and the viscosity of granular matter depend on the normal stress σ. Besides, the viscosity is proportional to the *inertial time* $t_i = \sqrt{\frac{m}{\sigma d}}$ built on the confining stress σ, the grain diameter d and their mass m. Introducing this time scale in the friction law provides a robust and generic description of dense granular flows [7, 10]. Combining the friction law (1) and the dilatancy

law (2), one can express the flow resistance of dry grains as a function of the solid fraction with no singularity when approching the maximum packing fraction, thereby avoiding the corresponding uncertainty:

$$\frac{\tau}{\sigma} \approx \mu_s + \frac{b}{c}(\phi_s - \phi). \tag{3}$$

Following such an approach for *immersed* particulate materials is quite promising. A significant step in this direction has been made by [4], in analyzing experimental immersed granular flow down an inclined plane. The flows were shown to satisfy a friction law similar to that of dry granular flows, see Eq. (1). In the limit of a negligible grain inertia, the time scale t of the friction law has been expressed from the new relevant physical parameters: the normal stress σ supported by the grains and the liquid viscosity η_0. The viscous time $t_v = 3\pi\frac{\eta_0}{\sigma}$ thus replaces the inertial time suitable for dry grains. Beyond this robust scaling, however, some questions still remains. First, in the presence of a liquid, no dilatancy law similar to Eq. (2), and hence no regular expression of the flowing resistance such as Eq. (3) has been identified yet. Second, one can expect that the details of the interaction between close particles in a liquid should have a significant effect on their collective behavior. In particular, some surface repulsion may be set into action between close enough particles. One can expect that it should limitate the magnitude of the lubrication interaction [13], and that the collective behavior should therefore be different whether or not most pairs of neighbouring particles approach sufficiently to set this surface repulsion into action [12].

In this paper, we study the flowing behavior of a dense suspension whose grains interact by viscous lubrication and possible repulsion. The study is based on *Soft Dynamics* simulations of the plane shear, prescribing the shear rate and the normal stress. We show that the steady flows of this dense suspension can be described by a friction and a dilatancy law, whose coefficients are found to depend on a key parameter of the grains: the distance below which surfaces repel each other. A simple scenario explaining these non-trivial dependencies is proposed, supported by the analysis of the local force distribution.

The paper is organized as follow: the material under consideration and the simulation method are described in section II, the collective response to shear is studied in section III and the internal processes underpinning the collective behavior are discussed in section IV.

II. SIMULATION OF A MODEL DENSE SUSPENSION WITH THE SOFT DYNAMICS

The *Soft Dynamics* method is a Discrete Element Method which we specifically developed to simulate the dynamics of dense suspensions. In this section, we briefly present its main features, especially the modes of interaction accounted: grain elasticity, lubrication and surface repulsion. More details can be found in our previous works [17–19].

Particles in a dense configuration interact with their close neighbours, with a typical surface-to-surface distance h much smaller than their own size d. They interact by viscous lubrication, which then dominates the hydrodynamic forces [see for instance 1]. Their surface may also interact directly with each other when they get close enough. This interaction can come from some electrostatic repulsion between surfactant molecules at the surface of bubbles or droplets (disjoining pressure). It may also reflect the size of surface asperities in the case of rough solid particles. In any case, under imposed normal stress σ, some surface repulsion will generate a typical equilibrium gap h_0 between neighbouring particles.

We chose to model this surface repulsion by a purely normal force in the form of a power law: $F_n^{dir} = \sigma d^2 \left(\frac{h}{h_0}\right)^{-p}$, with $p = 8$ as discussed in [17]. More generally, torques or tangential forces between surfaces could be included, as well as complex features such as solid friction, adhesion and interfacial visco-elasticity, depending on the nature of the particles under consideration. The normal and tangential lubrication force between both surfaces is expressed as [19]:

$$F_n^{vis} = \frac{3\pi\eta_0 a^4}{2h^3} v_n,\ F_t^{vis} = \frac{\pi\eta_0 a^2}{h} v_t, \tag{4}$$

where v_n and v_t are the normal and tangential relative surface velocities (which correspond to Poiseuille and Couette flow, respectively). Distance $a \approx \sqrt{d(h + |\delta_n|)}$ is the lateral extension of the gap region that mediates most of the lubrication force. Here, δ_n, is the normal component of the surface deflection $\vec{\delta}$ related elastically to the force: $Ea\vec{\delta} = \vec{F}^{ela} = \overrightarrow{F}^{vis} + \overrightarrow{F}^{dir}$, where E is essentially the Young's modulus of the bulk material. A cutoff value for the gap h is introduced as a way to avoid long range hydrodynamic interactions which are irrelevent to dense configurations: the particles interact only when $h < 0.4d$. Viscous and elastic torques are also included, as in [17].

The novelty of Soft Dynamics is to simulate the evolution of the elastic deflection $\vec{\delta}$ and of the twist angle for each pair of neighbouring particles and to take into account how they, in turn, affect the lubrication flow in the

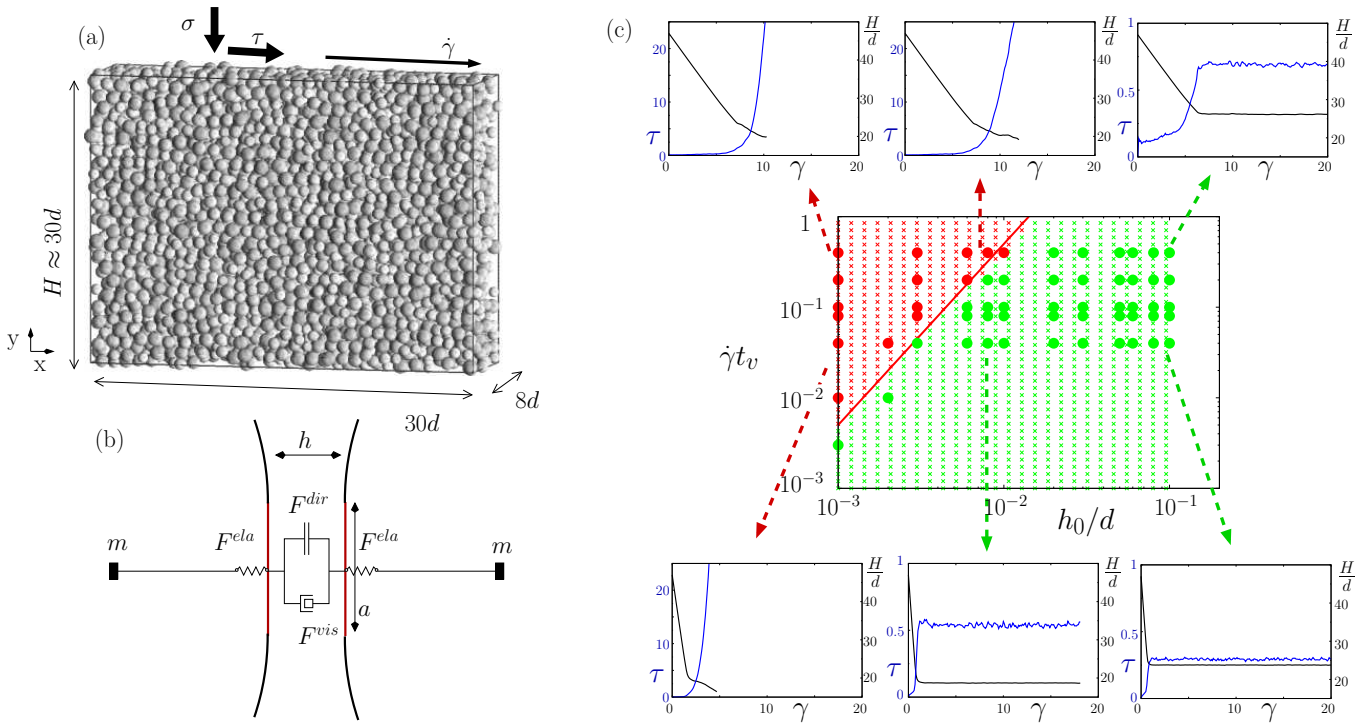

FIG. 1: (Color online) Plane shear of a dense particulate material immersed in a viscous liquid. (a) 5000 spheres, with a slightly polydisperse distribution ($d \pm 20\%$), are subjected to an imposed shear rate $\dot\gamma$ (imposed through Lees-Edwards boundary conditions) and a fixed normal stress σ in a fully periodic domain. To impose the normal stress, the target normal stress is set equal to σ at $t = 0$ and the height H of the simulation cell is set to evolve according to $M\,\ddot H = \sigma - \sigma_{yy}$, where σ_{yy} is the current normal stress and where M is a mass fixed at a value that corresponds to about one monolayer of particles. Observed normal stress fluctuations are small (less than 1%). (b) Interaction between two close elastic particles in a viscous fluid (see main text for detail). (c) Regimes of viscous (green color) and elastic (red) behaviours depending on the shear rate $\dot\gamma$ and the equilibrium gap h_0. The red line ($\dot\gamma t_v = 5000(h_0/d)^2$) empirically delimitates the two regimes. Large dots correspond to simulations with the whole sample. In six instances, an additional graph shows the shear stress τ (blue line, left axis) and the cell height H (black line,right axis) as a function of the shear deformation γ. Small crosses correspond to simulations of the separation of two particles with relative particle center velocity $\dot\gamma d$ and initial gap h_0.

$\kappa = \frac{\sigma}{E}$	h_0/d	$\dot\gamma t_v$
10^{-3}	$10^{-3} \to 10^{-1}$	$10^{-3} \to 4.10^{-1}$

TABLE I: Range of parameter investigated. The unit length, stress and time are the particle diameter $d = 1$, the normal stress $\sigma = 1$ and the viscous time $t_v = 3\pi\frac{\eta}{\sigma} = 1$. The particle mass is set low so that the inertial time is smaller than the viscous time, $t_i = \sqrt{\frac{m}{\sigma d}} = 0.1t_v$. The value of the stiffness number κ corresponds either to solid grains subjected to high normal stress ($E \approx 10^9$ Pa, $\sigma \approx 10^6$ Pa), or to the softer living cells, droplets or bubbles under lower stress ($E \approx 10^{4-5}$ Pa, $\sigma \approx 10^{1-2}$ Pa). The range of shear rates investigated corresponds to $10\,s^{-1} < \dot\gamma < 4.10^3\,s^{-1}$ for a viscosity close to that of water ($\eta = 10^{-3}$ Pa.s) and an applied normal stress 10^2 Pa $< \sigma < 4.10^4$ Pa, or for more viscous liquid ($\eta = 10$ Pa.s) and a normal stress 10^6 Pa $< \sigma < 4.10^8$ Pa.

inter-particle gap. As a result, the elastic, viscous and direct force/torque are balanced at the particle surfaces at all times. Correspondingly, the contributions to the stress $\boldsymbol{\sigma} = \frac{1}{V}\sum \overrightarrow{F} \otimes \overrightarrow{l}$, (where V is the volume of the sample, $\overrightarrow{F}$ the force transmitted between a pair of particles and $\overrightarrow{l}$ their center-to-center vector) arising from normal and tangential viscous forces as well as direct forces can be isolated: $\boldsymbol{\sigma} = \boldsymbol{\sigma^{dir}} + \boldsymbol{\sigma_n^{vis}} + \boldsymbol{\sigma_t^{vis}}$.

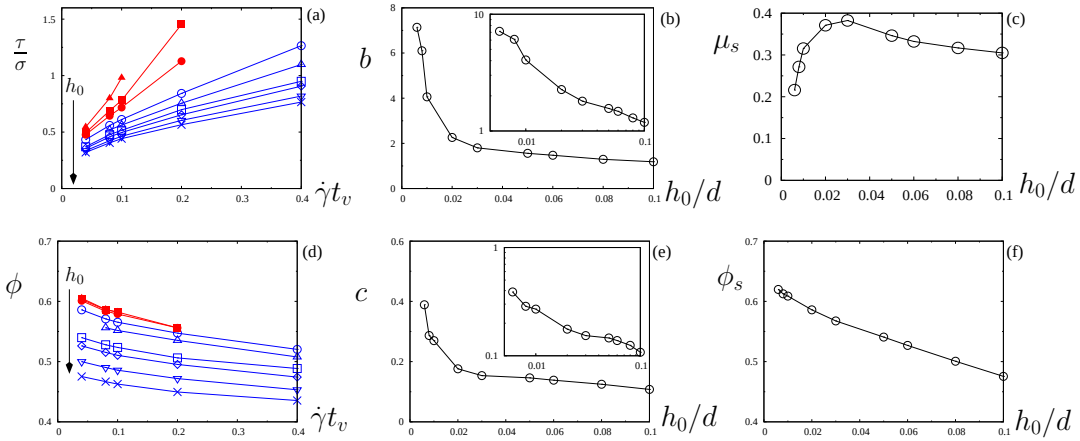

FIG. 2: (Color online) Mechanical behaviour of the simulated suspension as a function of the equilibrium gap: $h_0/d = 0.1$ ($\times$), 0.08 ($\triangledown$), 0.06 ($\Diamond$), 0.05 ($\square$), 0.03 ($\triangle$), 0.02 ($\circ$), 0.01 ($\bullet$), 0.008 ($\blacksquare$), 0.006 ($\blacktriangle$). (a) Friction law: shear stress τ versus shear rate $\dot{\gamma}$ for each value of h_0. (b) Corresponding slopes b (log-log plot in inset) and (c) y-intercepts μ_s of the linear fits $\frac{\tau}{\sigma} \approx \mu_s(h_0) + b(h_0)t_v\dot{\gamma}$. (d) Dilatancy law: solid fraction ϕ versus shear rate $\dot{\gamma}$ for each value of h_0. (e) Corresponding slopes c (log-log plot in inset) and (f) y-intercepts ϕ_s of the linear fits $\phi \approx \phi_s(h_0) - c(h_0)t_v\dot{\gamma}$.

III. COLLECTIVE RESPONSE TO SHEAR: IMPORTANCE OF SURFACE REPULSION

The numerical experiment consists in subjecting a sample of particles interacting as described in Section II to a shear, prescribing the normal stress σ and the shear rate $\dot{\gamma}$ (Fig. 1a,b). Both the normal stress σ and the Young's modulus E of the grains are fixed in all the simulations presented here. A value of the equilibrium gap h_0 is selected prior each run and is kept constant throughout the run. For each value of h_0, a series of runs with different values of the shear rate are performed. The range of parameters under investigation is presented in Table I. Each test starts from a loose configuration with no interaction or velocity. Both the normal stress and the shear rate are applied at the same time (see caption of Figure 1) and the stress within the simulation cell is measured as indicated above. Under the action of the normal stress, the simulation cell contracts, thus bringing the grains closer to each other. As they start interacting, the shear stress rises.

In the remaining of this work, we will describe and rationalize the observed behaviour with various degrees of detail, from macroscopic response to microstrucre properties. The macroscopic behaviour is shown by Fig. 1 (conditions for obtaining a steady flow), Fig. 2 (shear stress and dilatancy) and Fig. 3a (shear stress as a function of volume fraction). The relative importance of each type of force (lubrication versus direct forces due to surface repulsion) is shown by Fig. 4 and Fig. 3b (dominance of viscous versus direct forces). Microscopic data are presented through two types of statistics in Fig. 5 for each type of force (contributions by neighbour rank and angular distribution of contributions).

Steady flow *versus* elastic response. Because we impose the shear rate $\dot{\gamma}$ and allow for material dilatancy (we impose the normal stress σ rather than prescribing the volume), there is no jamming in the usual sense: the system always flows at low shear rates, and we measure an effective, dynamic friction coefficient, which may differ from its static counterpart. Although we do not observe jamming, the system exhibits two different behaviours (Fig. 1c), depending on the equilibrium gap h_0 and on the shear rate $\dot{\gamma}$. For low shear rates or large equilibrium gaps, the shear stress first increases and eventually reaches a steady value, which is similar to a viscous response. Conversely, for smaller equilibrium gaps or higher shear rates, the shear stress increases indefinitely, which is rather similar to an *elastic* response.

This peculiar collective response can be understood from the microscopic relaxation time at the particle scale. As discussed in [17], each pair of particles behaves like a non-linear Maxwell analogue. The prescribed shear rate tends to separate their centers at a typical velocity $\dot{\gamma}d$. If the shear rate is low enough with respect to the characteristic time of the equivalent Maxwell element, the particle surfaces have enough time to separate from each other (starting from their initial gap of order h_0) and the material tends to flow in a viscous manner. By contrast, if the flow is faster, many pairs of particle surfaces do not have enough time to get apart, hence the particles themselves deform and build large elastic forces. The material thus tends to respond elastically.

We tested this simple picture by simulating the separation of only two particles at a constant center-to-center velocity $\dot{\gamma}d$, from an initial surface-to-surface distance $h = h_0$ up to the cutoff distance $h = 0.4d$. The results of this test are plotted on Fig. 1c: small red crosses correspond to situations where the particles deform and the force

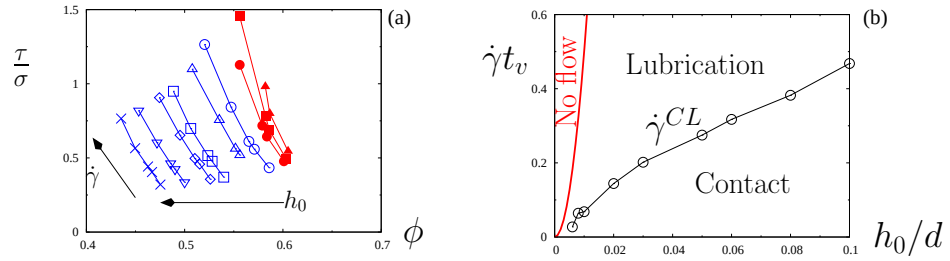

FIG. 3: (Color online) Two features of the steady flow behavior. (a) The shear stress τ can be expressed as a function of the solid fraction ϕ for each value of the equilibrium gap: $h_0/d = 0.1$ (×), 0.08 (▽), 0.06 (◊), 0.05 (□), 0.03 (△), 0.02 (○), 0.01 (•), 0.008 (■), 0.006 (▲). (b) Behaviour in terms of h_0 and $\dot{\gamma}$: elastic response (no flow, see Fig. 1c), dominant lubrication or dominant surface repulsion (see Sec. III).

increases continuously until the center-to-center distance reaches $1.4d$, while small green crosses represent situations where the force has started to relax by that time. Fig. 1c shows that the transition from viscous to elastic for one pair of particles coincides with the transition for the whole sample. It thus appears that the simple Maxwell picture at the two-particle level captures the existence of both macroscopic behaviours: steady flow and elastic response.

Friction law, dilatancy law: surface repulsion matters. In the steady regime, we observed that the stress, the shear rate and the solid fraction are homogeneous in the whole sample (there is no shear localisation), and that they display only weak time-fluctuations (about 1%). Figures 2a and d show the corresponding time-averaged value of the shear stress and of the solid fraction on 50 snapshots spanning a shear deformation of 5. To first order in $\dot{\gamma}$, for each value of the equilibrium gap h_0, the material satisfies a friction law and a dilatancy law of the form given by Eqs. (1) and (2). However, the corresponding parameters strongly depend on h_0: the slopes vary roughly like $b \propto (h_0/d)^{-2/3}$ and $c \propto (h_0/d)^{-1/2}$, and ϕ_s decreases almost linearly with h_0/d. As for μ_s, its dependence on h_0/d is not monotoneous: it reaches a maximun for $h_0/d \approx 0.03$, which is not far from the value for which, with the present value of σ/E, the surface deflection of particles become significant, (see [17, 18] for details).

Thus, one major result of this study is that such immersed particles behave just like dry grains with a rheological law that can be expressed in the form of Eq. (3), with no singularity in terms of the volume fraction. However, as shown by Figure 3a, the coefficients of this law depend on h_0. Thus, the solid fraction ϕ and the shear rate $\dot{\gamma}$ are not sufficient to predict the shear stress: a microscopic variable such as the equilibrium gap h_0 must be known in order to predict the flow behaviour of such immersed grains.

Viscous *versus* direct forces. Figure 4 shows the respective contributions of viscous forces and direct forces (due to surface repulsion) to the macroscopic stress in these steady flows. Several observations can be made. *(i)* Normal viscous forces (particle approach or separation) contribute much more than tangential viscous forces (sliding). That is consistent with Eq. (4) and with the dynamics of few particles in [19]. *(ii)* The viscous shear stress is approximately proportional to the shear rate, $\tau^{vis} \approx b^{vis}\dot{\gamma}$. Note that the corresponding slope varies roughly like $b^{vis} \simeq b_n^{vis} \propto (h_0/d)^{-2/3}$, just as the overall slope b. The slope b_t^{vis} for sliding depends more weakly on the equilibrium gap h_0. *(iii)* The contribution of surface repulsion, τ^{dir}, as opposed to that of viscous forces, does *not* vanish at small $\dot{\gamma}$ under such imposed normal stress conditions, see figure 4g; by contrast, if the volume was kept constant, it is anticipated that all forces (including surface repulsion) should scale linearly with the shear rate for small shear rates, see [13]. Hence, surface repulsion alone is responsible for the finite frictional flow threshold μ_s (which is the limit of τ/σ at small velocities). For illustration purposes, Figure 3c shows whether the macroscopic shear stress is dominated by surface repulsion or by lubrication. They contribute equally when the shear rate is given by $\dot{\gamma}^{CL} = \frac{\mu_s}{2b^{vis}-b} t_v$. This quantity happens to increase almost linearly with the equilibrium gap h_0. *(iv)* There is a tendency for the contributions of surface repulsion to the normal stress, σ^{dir} (and to a weaker extent to the shear stress, τ^{dir}), to *decrease* with the applied shear rate $\dot{\gamma}$.

Among the above results, points *(i)*, *(ii)* and *(iii)* are qualitatively not very surprising. By contrast, point *(iv)* does not have any straightforward interpretation in terms of macroscopic arguments. We shall therefore now examine local data to shed light on this apparent *loss* of contact.

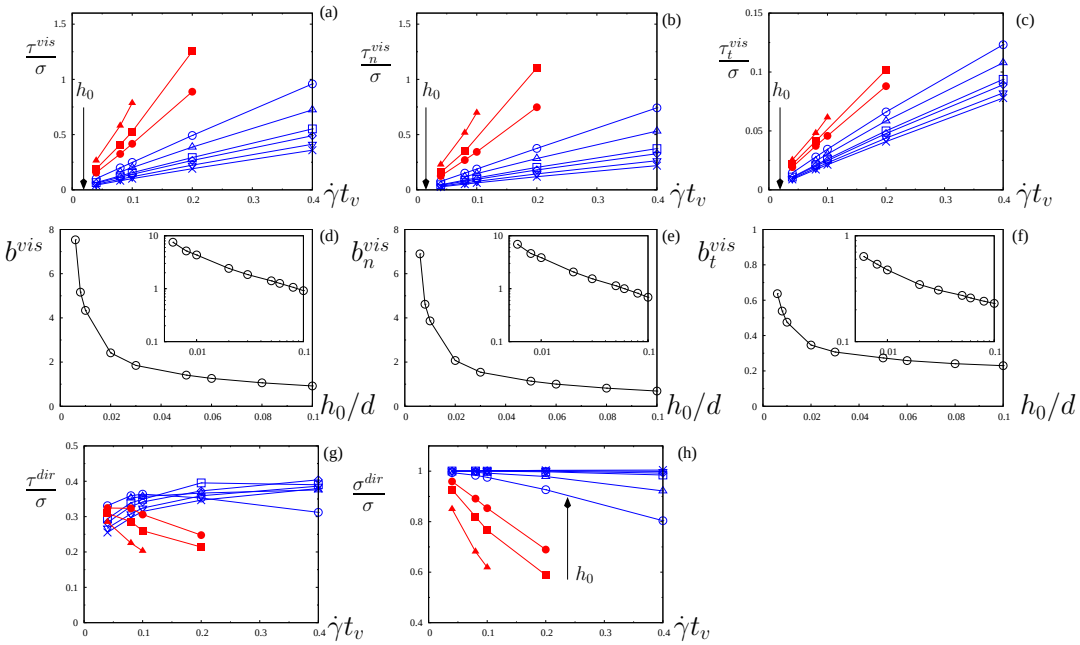

FIG. 4: (Color online) Contribution of viscous lubrication and surface repulsion to the stress. Symbols denote the equilibrium gap: $h_0/d = 0.1$ (×), 0.08 (▽), 0.06 (◇), 0.05 (□), 0.03 (△), 0.02 (○), 0.01 (●), 0.008 (■), 0.006 (▲). Shear stress supported by (a) all viscous forces (normal and tangential: τ^{vis}), (b) normal viscous forces (τ_n^{vis}) and (c) tangential viscous forces (τ_t^{vis}). (d–f) Corresponding slopes b^{vis} from the linear fits $\tau^{vis} \simeq b^{vis}\dot{\gamma}t_v$ (insets: log-log plots). (g,h) Shear stress τ^{dir} and normal stress σ^{dir} supported by the surface repulsion forces.

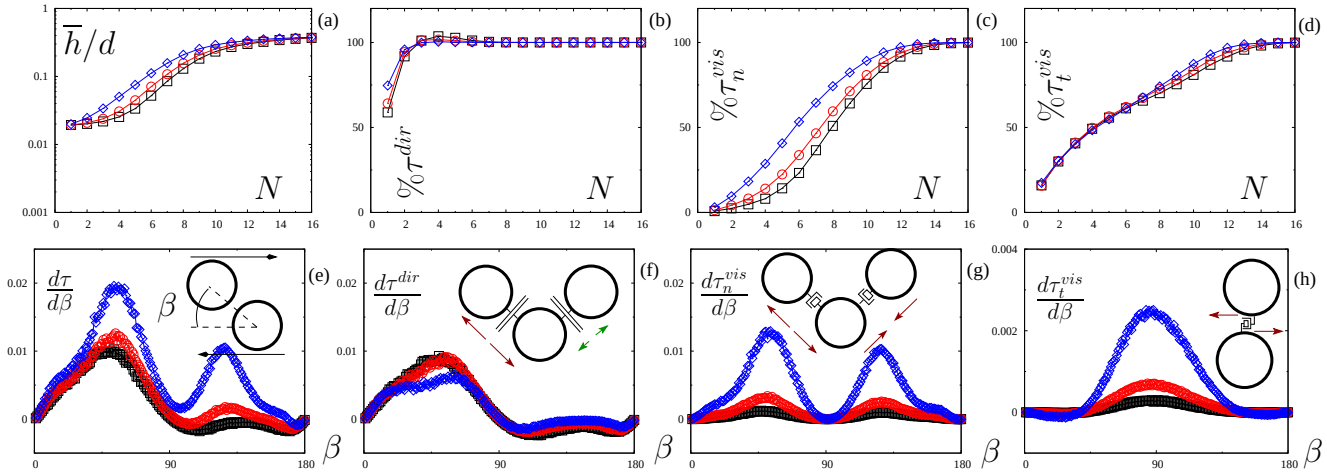

FIG. 5: (Color online) Microstructure of the steady flow. The statistical indicators presented here are averaged over 50 snapshots during a shear deformation of 5. Results correspond to one material (with $h_0 = 0.02d$) subjected to different shear rates $\dot{\gamma}t_v = 0.04$ (□), 0.1 (○) and 0.4 (◇). In graphs (a-d), $N = 1$ corresponds to an average over the closest gap of each particle, $N = 2$ to the second closest gaps, etc. (a) Average gap $\overline{h}$ for each value of N. (b) Cumulative distribution (in terms of N) of contributions to shear stress from surface repulsion forces. (c) Similar cumulative distribution for normal viscous forces. (d) Same distribution for tangential viscous forces. (e-h) Angular distribution $d\tau/d\beta$ of the shear stress mediated by pairs of grains with orientation β for each type of force.

IV. INTERNAL DYNAMICS AND RELATIVE GRAIN MOTION

In order to understand the apparent loss of contact between grains when the deformation rate is increased, let us examine the simulation data from the point of view of the surface-to-surface distance between neighbouring grains.

Unexpected stress contribution as a function of surface-to-surface distance. In order to test the influence of the surface-to-surface distance h, we have constructed several averaged quantities displayed in Figures 5a–d. To do that, we determined the closest neighbour of each grain (in terms of h) at all times. We used the corresponding pairs of grains to compute several averaged quantities labeled with $N = 1$. We then determined the neighbour of each grain with the next smallest value of the gap h and used it to compute values for $N = 2$, and so on.

Figure 5a displays the average h as a function of rank N: it ranges from $h \approx h_0$ for $N = 1$ to $h = 0.4d$ (interaction cutoff). The cumulative distribution displayed on Figure 5b shows that the shear stress arising from surface repulsion, τ^{dir}, is mediated almost totally by the first two closest neighbours, suggesting the existence of force chains as in dry granular flows. By contrast, Figures 5c–d show that as many as 10 neighbours contribute significantly to the viscous shear stress. That is rather counter-intuitive when considering that viscous forces vary very strongly with the gap h (see Eq. 4) and that the latter varies by one order of magnitude between the first and the tenth neighbour (see Figure 5a).

Angular distribution of stress contributions and relative grain motion. The surprisingly comparable viscous contribution from all first ten neighbours of each grain to the macroscopic shear stress indicates that mutual velocities and orientations of pairs of grains compensate for their gap variability. Therefore, we examined the angular distribution of the pairs of grains that contribute to the macroscopic shear stress. The angular distribution of the total shear stress, shown on Figure 5e, seems rather complex. But the decomposition into surface repulsion, normal and tangential force contributions, see Figures 5f–h, suggests a very simple microscopic scenario for each typical pair of neighbouring particles.

A pair of particles first approach each other around $\beta \approx 3\pi/4$, (the angle β is defined in the diagram of Figure 5e). As a result, for pairs oriented in this direction, surface repulsion and normal viscous forces both resist macroscopic shear and thus contribute positively, see Figures 5f–g. Once they have approached, both particles then slide around each other when $\beta \approx \pi/2$. At such an orientation normal forces (both surface repulsion and viscous forces) do not contribute to the macroscopioc shear stress, while tangential shear forces do contribute to it (see Figure 5h). When both particles depart, typically around $\beta \approx \pi/4$, surface repulsion helps this motion, hence the (weak) negative contribution in Figure 5f, while normal viscous forces again resist macroscopic shear, see Figure 5g. Such a scenario suggests that at low shear rates, the first few closest neighbours of a given particle are neither approaching nor separating, but are rather sliding, maintaining their surface-to-surface distance around $h \approx h_0$. Their contribution to τ_n^{vis} is then expected to be *smaller* than that of the next few neighbours, consistently with the lower slope in Fig. 5c for $N < 5$. Conversely, because they are currently sliding, their contribution to τ_t^{vis} is *higher* than that of the next few neighbours, see Fig. 5d for $N < 4$.

With the above microscopic scenario, the loss of contact observed in Figures 4g—h can now be understood as follows. While the normal stress σ tends to compress pairs of grains of all orientations, the shear stress τ is compressive in some directions (around $\beta \approx 3\pi/4$ in the notations of Fig. 5e) and tensile in other directions ($\beta \approx \pi/4$). As the shear rate is increased, one might naively think that all velocities and viscous forces are increased and that typical particle trajectories should not be altered. But in fact, the present imposed normal stress conditions imply that the ratio of the shear stress and normal stress τ/σ increases when the shear rate is increased. Hence, tensile forces within particle pairs become more frequent as compared to compressive forces. That explains why the average surface-to-surface distance increases with velocity (as observed in Fig. 5a) and why the stress supported by direct forces decreases at high shear rate in Figures 4g–h. This *loss of contact* is more significant for small values of the equilibrium gap h_0.

V. CONCLUSION

The flowing behavior of the present model dense suspension appears to satisfy a friction law and a dilatancy law, similar to those of dry grains. Likewise, the shear to normal stress ratio developed in steady flow are a regular function of the solid fraction (see Eq.3), with no singularity at maximum packing. The coefficients involved in these laws depend on the surface repulsion through the equilibrium gap h_0 (see Figure 3a).

A closer look at the microscopic data in the simulation has revealed that a simple scenario (see Fig. 5e–h) captures much of the microscopic distribution of the overall shear stress. In particular, it appears (see Figures 5c–d) that in such a dense, lubricated system, most forces transmitted to neighbouring particles are comparable: locally, particle pairs appear to exchange an imposed force rather than to move at an imposed relative velocity: in a sense, the lubrication film extends each particle in such a way that it is in effective mechanical contact with its neighbours, thus

building a much more robust force network than in a dry granular material.

[1] Ball, RC & Melrose, JR 1997 A simulation technique for many spheres in quasi-static motion under frame-invariant pair drag and Brownian forces. *Physica A: Statistical and Theoretical Physics* **247** (1-4), 444–472.

[2] Bertevas, E., Fan, X. & Tanner, R.I. 2010 Simulation of the rheological properties of suspensions of oblate spheroidal particles in a Newtonian fluid. *Rheologica acta* **49** (1), 53–73.

[3] Brady, J.F. & Bossis, G. 1985 The rheology of concentrated suspensions of spheres in simple shear flow by numerical simulation. *Journal of Fluid Mechanics* **155**, 105–129.

[4] Cassar, C., Nicolas, M. & Pouliquen, O. 2005 Submarine granular flows down inclined planes. *Phys. Fluids* **17**, 103301.

[5] Coussot, P. 2005 *Rheometry of pastes, suspensions, and granular materials*. Wiley-Interscience.

[6] Coussot, P. 2007 Rheophysics of pastes: a review of microscopic modelling approaches. *Soft Matter* **3** (5), 528–540.

[7] da Cruz, F., Emam, S., Prochnow, M., Roux, J-N. & Chevoir, F. 2005 Rheophysics of dense granular materials: Discrete simulation of plane shear flows. *Phys. Rev. E* **72**, 021309.

[8] Dratler, DI & Schowalter, WR 1996 Dynamic simulation of suspensions of non-Brownian hard spheres. *Journal of Fluid Mechanics* **325**, 53–77.

[9] Forterre, Y. & Pouliquen, O. 2008 Flows of Dense Granular Media. *Annu. Rev. Fluid Mech.* **40**, 1.

[10] GDR MiDi 2004 On dense granular flows. *Euro. Phys. J. E* **14**, 341–365.

[11] Huang, N. & Bonn, D. 2007 Viscosity of a dense suspension in Couette flow. *J. Fluid Mech.* **590**, 497–507.

[12] Huang, N., Ovarlez, G., Bertrand, F., Rodts, S., Coussot, P. & Bonn, D. 2005 Flow of Wet Granular Materials. *Phys. Rev. Lett.* **94** (2), 28301.

[13] Lemaître, A., Roux, J.N. & Chevoir, F. 2009 What do dry granular flows tell us about dense non-Brownian suspension rheology? *Rheologica Acta* **48** (8), 925–942.

[14] Mewis, J. & Wagner, N.J. 2009 Current trends in suspension rheology. *Journal of Non-Newtonian Fluid Mechanics* **157** (3), 147–150.

[15] Morris, J.F. 2009 A review of microstructure in concentrated suspensions and its implications for rheology and bulk flow. *Rheologica acta* **48** (8), 909–923.

[16] Ovarlez, G., Bertrand, F. & Rodts, S. 2006 Local determination of the constitutive law of a dense suspension of noncolloidal particles through magnetic resonance imaging. *J. Rheol.* **50**, 259.

[17] Rognon, P., Einav, I. & Gay, C. 2010 Internal relaxation time in immersed particulate materials. *Phys. Rev. E* **81**, 061304.

[18] Rognon, P. & Gay, C. 2008 Soft Dynamics simulation. 1. Normal approach of two deformable particles in a viscous fluid and optimal-approach strategy. *Euro. Phys. J. E* **27**, 253–260.

[19] Rognon, P. & Gay, C. 2009 Soft Dynamics simulation. 2. Elastic spheres undergoing a T1 process in a viscous fluid. *Euro. Phys. J. E* **30**, 291–301.

[20] Rognon, P.G., Roux, J.N., Naaim, M. & Chevoir, F. 2008 Dense flows of cohesive granular materials. *J. Fluid Mech.* **596**, 21–47.

[21] Stickel, J.J. & Powell, R.L. 2005 Fluid mechanics and rheology of dense suspensions. *Annu. Rev. Fluid Mech.* **37** (1), 129–149.